bioRxiv preprint doi: https://doi.org/10.1101/718155; this version posted July 29, 2019. The copyright holder for this preprint (which was not certified by peer review) is the author/funder, who has granted bioRxiv a license to display the preprint in perpetuity. It is made available under aCC-BY 4.0 International license.

High throughput competitive fluorescence polarization assay reveals functional redundancy in the S100 protein family

The specificity map of S100 interactions

Márton A. Simon[1], Péter Ecsédi[1], Gábor M. Kovács[2], Ádám L. Póti[3], Attila Reményi[3], József Kardos[1], Gergő Gógl[1,4*] and László Nyitray[1*]

[1]Department of Biochemistry and [2]Department of plant anatomy, Institute of Biology, Eötvös Loránd University, 1117 Budapest, Hungary

[3]Institute of Organic Chemistry, Research Center for Natural Sciences, Hungarian Academy of Sciences, 1117 Budapest, Hungary

[4]Equipe Labellisee Ligue 2015, Department of Integrated Structural Biology, Institut de Genetique et de Biologie Moleculaire et Cellulaire (IGBMC), INSERM U1258/CNRS UMR 7104/Universite de Strasbourg, 1 rue Laurent Fries, BP 10142, F-67404 Illkirch, France

*To whom correspondence should be addressed: Gergő Gógl: +33 7 69729949, goglg@igbmc.fr; László Nyitray: +36 1 3722500 ext 8783, nyitray@elte.hu

bioRxiv preprint doi: https://doi.org/10.1101/718155; this version posted July 29, 2019. The copyright holder for this preprint (which was not certified by peer review) is the author/funder, who has granted bioRxiv a license to display the preprint in perpetuity. It is made available under aCC-BY 4.0 International license.

Abstract

The calcium-binding, vertebrate-specific S100 protein family consists of 20 paralogs in humans (referred as the S100ome), with several clinically important members. To assess their interactome, high-throughput, systematic analysis is indispensable, which allows one to get not only qualitative but quantitative insight into their protein-protein interactions (PPIs). We have chosen an unbiased assay, fluorescence polarization (FP) that revealed a partial functional redundancy when the complete S100ome (n=20) was tested against numerous model partners (n=13). Based on their specificity, the S100ome can be grouped into two distinct classes: promiscuous and orphan. In the first group, members bound to several ligands (>4-5) with comparable high affinity, while in the second one, the paralogs bound only one partner weakly, or no ligand was identified (orphan). Our results demonstrate that *in vitro* FP assays are highly suitable for quantitative ligand binding studies of selected protein families. Moreover, we provide evidence that PPI-based phenotypic characterization can complement the information obtained from the sequence-based phylogenetic analysis of the S100ome, an evolutionary young protein family.

Author summary

Functional similarity among a protein family can be essential in order to understand proteomic data, to find biomarkers, or in inhibitor design. Proteins with similar functions can compensate the loss-of-function of the others, their expression can co-vary under pathological conditions, and simultaneous targeting can lead to better results in the clinics. To investigate this property one can use sequence-based approaches. However, this path can be difficult. In the case of the vertebrate specific, evolutionary young, S100 family, phylogenetic approaches lead to ambiguous results. To overcome this problem, we applied a high-throughput biochemical approach to experimentally measure the binding affinities of a large number of S100 interactions. We performed unbiased fluorescence polarization assay, involving the complete human S100ome (20 paralogs) and 13 known interaction partners. We used this measured 20x13 (260) protein-protein interaction array to reveal the functional relationships within the family. Our work provide a general framework for studies focusing on phenotype-based domain classification.

Introduction

Biochemical characterization of protein-protein interactions (PPIs) is a challenging field in molecular life sciences, which is usually limited to the determination of steady state dissociation constants [1]. The accurate determination of thermodynamic parameters of molecular interactions is performed by fast, but superficial high-throughput (HTP) methods. In the literature several HTP approaches are applied such as co-immunoprecipitation [2], yeast two hybrid and spot assays [3], pull-down assay [4], holdup assay [5] and direct fluorescence polarization/anisotropy [6]. In direct fluorescence polarization (FP) experiments, a fluorescent probe (usually a labeled peptide) is titrated with a globular partner. Their association is monitored by the polarization of the emitted light of the fluorophore (Fig 1A). In a

bioRxiv preprint doi: https://doi.org/10.1101/718155; this version posted July 29, 2019. The copyright holder for this preprint (which was not certified by peer review) is the author/funder, who has granted bioRxiv a license to display the preprint in perpetuity. It is made available under aCC-BY 4.0 International license.

modified FP experiment called competitive assay, both the probe and partner concentration are fixed, and the reaction mixture is titrated with an unlabeled competitor molecule (peptide or protein). Depolarization of the emitted light is indicative of the competition between the probe and the competitor in binding to the partner (Fig 1BC). While direct FP can be perturbed by the presence of the fluorescent dye, the competitive assay is unbiased and therefore more suitable for accurate HTP measurements of dissociation constants [7,8].

S100 proteins belong to the superfamily of EF-hand containing calcium-binding proteins. They appeared in early vertebrates and consist of 20 core paralogs in the human proteome [9]. S100s are associated with several disease conditions, such as cardiomyopathies, cancer, inflammatory and neurodegenerative diseases, in which overexpression of S100 proteins can be observed in the affected cells [10–12]. Due to this reason, they are emerging bio-markers and also promising therapeutic targets [13]. Despite their growing importance, the literature still lacks their comprehensive and systematic analysis, which would be essential for developing rational strategies for drug development. Similarly to calmodulin, they can interact with protein or peptide targets in a calcium-dependent manner [14]. They are generally considered as relatively low specificity proteins, with dozens of interaction partners, among them they are unable to maintain a high selectivity [15]. In this study we determined the interaction profile of the full human S100 family (termed here as the S100ome) against a set of diverse known S100 partners (and some of their paralogs) systematically, including kinases such as RSK1 [16] and its paralogs MK2 and MNK1; cytoskeletal elements such as CapZ [17] (commonly known as TRTK12), NMIIA [18], ezrin [19], FOR20 and its paralog FOP [20]; membrane proteins such as NCX1 [15] and TRPM4 [21]; and other signaling proteins such as the tumor suppressor p53 [22–24], SIP [15] and MDM4 [23].

Results

Mapping the S100ome with FP measurements

The interactions between S100 homodimers and their selected labeled peptide partners were studied first by direct FP assay (Fig S1-13.). We have found that all reasonable S100 interactions gave an experimental window of 50-200 mP (polarization). If significant binding was detected (Kd < 200 µM) between a labeled peptide and an S100 protein, a subsequent competitive FP assay was performed. In cases, where no labeled peptide was available (e.g. when globular protein domains were used as competitors), we used non-cognate tracers against all possible S100 proteins. Additionally, we tested the possible binding between these competitors and the non-cognate probes in direct FP experiments to eliminate the possibility of re-binding (Fig S14.). This way, we tested 180 unique direct and 150 unique competitive interactions and found 89, and 66 significant interactions, respectively (Table 2., Fig S1-13.).

As mentioned previously, competitive FP provides unbiased (or more specific) affinities, unaffected by the chemical labeling, making it a better tool to measure protein-protein interactions (Fig 2AB). Nevertheless, there are some pitfalls (Fig 2.), which should be taken into consideration while analyzing competitive data. First of all, the experimental window of the competitive measurement should be the same as the experimental window of the direct measurement (Fig 2C). Studying large biomolecules (e.g. globular proteins) in a competitive experiment often results in an increased base polarization (P_{min}) due to the change in biophysical properties of the reaction mixture (e.g. change in viscosity). Moreover, during a competition experiment, it is possible that the competitor can interact

bioRxiv preprint doi: https://doi.org/10.1101/718155; this version posted July 29, 2019. The copyright holder for this preprint (which was not certified by peer review) is the author/funder, who has granted bioRxiv a license to display the preprint in perpetuity. It is made available under aCC-BY 4.0 International license.

with the probe itself, which can also cause an increase in the base polarization (Fig S14.). In rare cases, saturation polarization can be also altered. Additionally, experimental artifacts of unknown origin can be observed occasionally (Fig 2D). Here, a sharp decline can be detected during the titration, which results in an IC50 value smaller than the fixed receptor concentration. This observed sub-stoichiometric complex formation should be handled with extra care as it is likely due to unexpected biophysical phenomena, such as protein aggregation. To standardize and automatize data handling and to eliminate subjective factors, we developed a Python-based universal program, called ProFit for fitting all direct and competitive experimental data (freely available at https://github.com/GoglG/ProFit).

Validation with ITC measurements

The biochemically described S100 binding motifs, found in the literature, show an extremely low sequence similarity [15,23] (Fig 3A). Mostly linear segments are recognized by the human S100ome, however, no consensus S100 binding sequence can be defined[15]. In general, hydrophobic residues are preferred, but additional basic residues can also be favored in some instances. Moreover, S100 proteins can form two types of complexes (Fig 3B). Earlier studies showed that a symmetric S100 dimer can recognize two identical binding motifs, symmetrically [17,25,26]. In recent studies however, several asymmetric complexes were also described [18,27,28]. In those cases, an S100 dimer captures a single straddling the two binding sites. As the binding affinity highly depends on the stoichiometry of the interaction, we selected a set of significant, peptide-based interactions for isothermal titration calorimetric (ITC) measurements. This way, we validated the interactions that were originally detected by the FP assay and determined the binding stoichiometry in all instances.

All determined K_d values correlated well with the data provided by the orthogonal FP measurements (Table 3., Fig S15.). Symmetric interactions were found with CapZ, NCX1, SIP, TRPM4 and MDM4. In cases of CapZ and MDM4, the experimental data was fitted by a two binding site model indicating slightly different affinities and a complex relationship between the S100 monomers. In contrast, asymmetrical interactions were detected with p53, RSK1, C-ERMAD, NMIIA and FOP. These findings confirmed the expected binding stoichiometry in all cases and clarified the binding mode of TRPM4 and FOP. We hypothesize that the binding mode of close paralogs should be identical (symmetric or asymmetric), therefore, asymmetric binding was assumed for MNK1, MK2 (based on RSK1) and FOR20 (based on FOP). We performed these ITC measurements in parallel with the FP experiments and based on the refined stoichiometry, monomer or dimer S100 concentrations were used during the FP data evaluation.

Specificity map of the S100ome

The 20 S100 paralogs, whose interactions were studied here, represent almost the complete human S100ome [13]. It is a Chordata-specific, evolutionary young protein family, and despite the fact that they exhibit moderate sequence similarity, they are structurally very similar owing to their small size (~100 residues) and conserved fold (including two consecutive EF hand motifs) (Fig S16.). Due to this reason, their phylogenetic analysis generally does not lead to unambiguous results [29,30]. Applying different parameters during the analyses resulted in varied grouping of the human S100ome, moreover only a few clades received statistical supports (see our analyses in Fig S17.). Because of these ambiguities of the phylogenetic analyses, a phenotypic screening and analysis could provide a more reliable grouping and could reveal functional similarities among the paralogs of the protein family of interest beside the sequence-based genealogies. For such purpose, we decided to create a robust phenogram [31], representing the functional relationships within the human S100ome, using

bioRxiv preprint doi: https://doi.org/10.1101/718155; this version posted July 29, 2019. The copyright holder for this preprint (which was not certified by peer review) is the author/funder, who has granted bioRxiv a license to display the preprint in perpetuity. It is made available under aCC-BY 4.0 International license.

hierarchical clustering (UPGMA) [32]. This analysis separated the S100ome into two groups, in which the first group contains S100 proteins generally lacking significant interactions (termed here as "orphan" S100 proteins) and the second group comprises generally good binders (termed here as "promiscuous" S100 proteins) (Fig 4.). While promiscuous S100 proteins showed significant binding to at least a few (4-5) of the tested interaction partners, orphan S100 proteins showed either no sign of partner binding, or a weak binding to a single partner.

Discussion

Competitive FP as a potent tool to measure high-throughput macromolecular interactions

Although numerous HTP, semi-quantitative approaches are available and many low-throughput but highly accurate methods exist to measure PPIs, reliable, quantitative HTP methods are scarce in the literature. On the one hand, direct FP assay can be performed in large scale in multi-well plates which makes it an ideal method for rapid interaction screening, however, it has the serious limitation of chemical labeling that can perturb the binding measurement. Competitive FP, on the other hand, shares the same properties but without any possible interference from the labeling dye. Moreover, it provides comparative results to other, orthogonal, usually low-throughput, label-free biochemical assays, such as ITC or SPR measurements [33]. In summary, competitive FP assay is robust and HTP, thus it is a valuable tool for screening macromolecular interactions involving linear peptide motifs, RNA/DNA oligonucleotides or fluorescent small molecules [34,35].

Evidence for functional redundancy within the S100 family and possible functions of the orphan group

S100 proteins are usually considered as ‘sticky’, relatively low specificity proteins [15], however no systematic study has been performed to make a specificity map involving the complete S100ome. Usually, the tested S100 proteins only covered the closest relatives (e.g. S100A2, S100A4, S100A6, S100B, S100P), and the results often showed redundant bindings [19,27,36–38]. Based on functional clustering, we have revealed here that the S100ome can be separated into two groups. The minor group of 8 members includes promiscuous paralogs, with a clear sign of functional redundancy. However, this does not mean that they do not have specific interactions (for example, RSK1 is highly specific partner of S100B) In contrast, the major group consists of 12 members without a clear binding preference. The function of this orphan group on the molecular level is less defined, although all S100 proteins (with the exception of S100A10) are at least involved in calcium homeostasis. They may represent intra- and perhaps also extracellular calcium ion buffers (without specific interaction partners) or they can have highly specific, yet undiscovered interaction partners [39]. As an example, S100A10, the only S100 protein without a functional EF hand motif, can mediate a very high affinity, and rather specific interaction with annexin A2 [37]. As a third scenario, it is still possible that there is functional redundancy within the orphan group, but our knowledge about S100 interaction partners is more limited in this group compared to the promiscuous group. Moreover, the present study covered only S100 homodimers (and the S100G monomer), although some S100 proteins can form heterodimers [40]. As an example, the S100A8/A9 (both coming from the orphan group) can form a functional heterodimer with known interaction partners [41].

bioRxiv preprint doi: https://doi.org/10.1101/718155; this version posted July 29, 2019. The copyright holder for this preprint (which was not certified by peer review) is the author/funder, who has granted bioRxiv a license to display the preprint in perpetuity. It is made available under aCC-BY 4.0 International license.

Function-based examination of relationships within the S100ome complements phylogenetic analysis

The phylogenetic analyses of the human S100ome resulted in rather ambiguous genealogies, likely due to the young age of the protein family (Fig S17.). Nevertheless, the clade including S100A2, S100A3, S100A4, S100A5, S100A6 was supported with high statistical values in all analyses (Fig S17.), similarly as it had also been found by others [29,30]. Our functional analysis has revealed that all members of this clade belong to the same subset of the promiscuous group, with a greatly similar functional profile. However, the phylogeny of the rest of the S100ome is supported with lower statistical values. Therefore, we suggest that in such scenarios, function-based phenotypic clustering can complement the information obtained from pure sequence-based phylogenetic analysis [42]. In our case, the S100 family can be divided, relatively unambiguously, into two bigger clusters, thus giving a more robust classification. Mapping the specificity and clustering of the S100ome contribute to the better understanding of this vertebrate-specific Ca^{2+}-binding protein family. An implication of the functional redundancy defined hereby is a possibility that a function-based combinatorial S100-biomarker strategy may be more effective than detecting individual proteins.

Materials and methods

Expression and purification of S100 proteins. Protein preparations were done as described previously [43]. Briefly, the cDNAs of S100 proteins were cloned into a modified pET15b expression vector. All protein constructs were expressed in *Escherichia coli* BL21 (DE3) cells (*Novagen*) with a *Tobacco Etch Virus* (TEV) cleavable N-terminal His_6-tag, and purified by Ni^{2+} affinity chromatography. The His_6-tag was cleaved by TEV protease, which was followed by either hydrophobic interaction chromatography, ion exchange chromatography or size-exclusion chromatography with applying standard conditions [43]. The quality of the recombinant proteins were checked by SDS-PAGE analysis.

Expression and purification of kinases. The kinase domains, MK2 (1-400) and MNK1 (1-465) were cloned into a variant pGEX expression vector. The kinase domains were expressed in *Escherichia coli* ROSETTA (DE3) cells (*Novagen*) with TEV cleavable N-terminal GST and a non-cleavable C-terminal His_6-tag. The recombinant proteins were purified using Ni^{2+} and GST affinity purification. The quality of the kinase domains was checked by SDS-PAGE analysis. FP measurements were performed without cleavage of the GST tag.

Expression and purification of recombinant peptides. The peptides FOR20 (1-48), FOP (1-48), p53 (1-60; 17-53), NMIIA (1894-1937), C-ERMAD (516-560 and 516-586) and RSK1 (696-735 and 689-735) were expressed in *Escherichia coli* BL21 (DE3) cells (*Novagen*) with TEV-cleavable N-terminal GST-tag, and purified by GST affinity chromatography. The tag was cleaved by TEV protease. After cleavage, the TEV protease and GST tag were eliminated by heat denaturation and centrifugation. The supernatant was purified by RP-HPLC using a Jupiter 300 Å C_5 column (*Phenomenex*). The quality of the expressed peptides was checked by mass spectrometry (MS).

Peptide synthesis. The CapZ (265-276), NCX1 (254-265), SIP (188-202), TRPM4 (129-147) and MDM4 (25-43) peptides were chemically synthesized using solid phase peptide synthesis (PS3 peptide synthesizer, *Protein Technologies*) with Fmoc/*t*Bu strategy in the case of (5(6)-carboxyfluorescein)

bioRxiv preprint doi: https://doi.org/10.1101/718155; this version posted July 29, 2019. The copyright holder for this preprint (which was not certified by peer review) is the author/funder, who has granted bioRxiv a license to display the preprint in perpetuity. It is made available under aCC-BY 4.0 International license.

labeled and unlabeled version. Peptides were purified by RP-HPLC using a Jupiter 300 Å C_{18} column (*Phenomenex*). The quality of the peptides was monitored by HPLC-MS.

Determination of concentrations. Concentrations of peptides and proteins were determined by UV-spectrophotometry using the absorbance of Tyr and Trp residues. In the absence of these aromatic residues, the concentrations were calculated by using the absorbance of the compound on 205 and 214 nm [44,45].

Fluorescence labeling. Chemically synthesized peptides (CapZ, NCX1, SIP, TRPM4, MDM4) were labeled with 5(6)-carboxyfluorescein at the N-terminus at the end of the synthesis. The recombinant peptides (p53, NMIIA and RSK1) were labeled with fluorescein-isothiocyanate at an N-terminal Cys residue using the protocol described previously [43]. C-ERMAD was labeled by Alexa Fluoro 568 C_5 maleimide [19]. The excess labeling agent was eliminated by using Hitarp desalting column (*GE Healthcare*). The labeled peptides were further purified and separated from the unlabeled peptides by RP-HPLC using a Jupiter 300 Å C_5 column (*Phenomenex*). The concentration of fluorescent peptides and the efficiency of labeling were determined by measuring the absorbance of the fluorescent dye and the peptides.

FP measurements. Fluorescence polarization was measured with a Synergy H4 plate reader (*BioTek Instruments*) by using 485 ± 20 nm and 528 ± 20 nm, and 530 ± 25 nm and 590 ± 35 nm band-pass filters (for excitation and emission, respectively) in cases of fluorescein-based (former) and Alexa Fluoro 568-based (latter) measurements. In direct FP measurements, a dilution series of the S100 protein was prepared in 96 well plates (Tomtec plastics, PP0602; or 4titude, 96 well skirted pcr plate, 4ti-0740) in a buffer that contained 150 mM NaCl, 20 mM HEPES pH 7.5, 1 mM $CaCl_2$, 0.5 mM TCEP, 0,01% Tween20 and 50 nM fluorescent-labeled peptide (probe). The volume of the dilution series was 50 µl, which was later divided into three technical replicates of 15 µl during transferring to 384 well micro-plates (Greiner low binding microplate, 384 well, E18063G5). In total, the polarization of the probe was measured at 8 different S100 concentrations (whereas one contains no S100 protein and corresponds to the free peptide). In competitive FP measurements, the same buffer was supplemented with S100 proteins to achieve a complex formation of 60-80%, based on the titration. Then, this mixture was used for creating a dilution series of the competitor (e.g. unlabeled peptide, or purified protein) and the measurement was carried out identically as in the direct experiment. Competitive FP measurement was executed if the fitted K_d value originated from the direct FP titration was below 200 µM. Table 1. shows the peptides used for direct and competitive FP measurements. The typical experimental window of an S100 interaction was found to be around 100 mP (polarization). However, some direct titration caused marginally small change in the polarization signal (10-30 mP), that we decided not to analyze further.

Fitting of FP data. The K_d of the direct and competitive FP experiment was obtained by fitting the measured data with quadratic and competitive equation, respectively *[7]*. For automatic fitting, we used an in-house developed, Python-based program, called ProFit, which is available as a supplement of this article (see data availability section). The program is capable to process multiple experimental data at once, evaluate direct-competitive experimental data series pairs and estimate the variance of the deduced parameters (e.g. dissociation constants) through a Monte Carlo approach. It produces ready to use figures for publications, as well as a report sheet for evaluation.

bioRxiv preprint doi: https://doi.org/10.1101/718155; this version posted July 29, 2019. The copyright holder for this preprint (which was not certified by peer review) is the author/funder, who has granted bioRxiv a license to display the preprint in perpetuity. It is made available under aCC-BY 4.0 International license.

ITC measurements. Titrations were carried out either at 310 or 298 K in a buffer containing 150 mM NaCl, 20 mM HEPES pH 7.5, 1 mM $CaCl_2$, 0.5 mM TCEP, using a MicroCal PEAQ-ITC instrument. The acquired data were fitted by PEAQ-ITC analysis software using the model "One Set of Sites" for most of the experiments, however for S100B-CapZ and S100B-MDM4 this model provided unsatisfactory fits and the model "Two Sets of Sites" were applied instead. Note that we used the minimal interacting region (696-735) of RSK1 instead of the larger construct (689-735), which was used in the direct FP assay.

Bioinformatical analysis. For the phylogenetic analysis, the human S100 protein sequences were aligned using ClustalW [29] (gap open penalty 10 and gap extension penalty 0.1 for pairwise alignment, gap open penalty 10 and gap extension penalty 0.2 for multiple sequence alignment, BLOSUM weight matrix), Kalign [46], MAFFT [47] (E-INS-i strategy, BLOSUM62 scoring matrix, 1.53 gap opening penalty without offset value), Muscle [46], Prank [46] and T-Coffe [46] algorithms. Gaps were replaced by ambiguous residues (question marks) before the beginning and after the end of each sequence in the raw sequence alignment to avoid the over-interpretation of the highly variant tail extensions in the further analysis. Phylogeny was conducted with RaxML GUI [48]. Evolutionary history was inferred using maximum likelihood algorithm with ProtGamma and LG as substitution model and substitution matrix, respectively [49], with 10 runs and 1000 bootstrap replicates. For the mapping of functional relationships and clustering, the dendrogram from the S100ome data set was constructed using the unweighted pair-group method with arithmetric average (UPGMA) method [32] based on the Euclidean distance using the PAST software [50].

Acknowledgement

We would like to thank Dániel Knapp form the Department of Plant Anatomy, ELTE for the help in bioinformatical analyses. This work was supported by the National Research Development and Innovation Fund of Hungary (K 119359 to L.N. K120391 to J.K.). M.A.S. and G.G. were supported through the New National Excellence Program of the Hungarian Ministry of Human Capacities (ÚNKP-18-2 and ÚNKP-18-3, respectively). We also acknowledge the FIEK_16-1-2016-0005, VEKOP-2.3.3-15-2016-00011 grants and Project no. 2018-1.2.1-NKP-2018-00005 implemented with the support provided from the National Research, Development and Innovation Fund of Hungary, financed under the FIEK_16, VEKOP-2.3.3-15-2016 and 2018-1.2.1-NKP funding schemes, respectively. G.G. was supported by the Post-doctorants en France program of the Fondation ARC.

Data availability

The computer code produced for this study is available in the following website.

- ProFit: GitHub (https://github.com/GoglG/ProFit)

Author Contributions

M.A.S. carried out the experiments, analyzed the experimental data and wrote the paper. G.G. and L.N. supervised the research, analyzed the data and wrote the paper. P.E., J.K., G.M.K. Á.L.P. and A.R. contributed by carrying out protein and peptide expression, ITC experiments and bioinformatical analyses.

bioRxiv preprint doi: https://doi.org/10.1101/718155; this version posted July 29, 2019. The copyright holder for this preprint (which was not certified by peer review) is the author/funder, who has granted bioRxiv a license to display the preprint in perpetuity. It is made available under aCC-BY 4.0 International license.

Conflict of Interest

The authors declare no conflict of interest.

References

1. Zhou M, Li Q, Wang R. Current Experimental Methods for Characterizing Protein-Protein Interactions. ChemMedChem. 2016;11: 738–756. doi:10.1002/cmdc.201500495

2. Xing S, Wallmeroth N, Berendzen KW, Grefen C. Techniques for the analysis of protein-protein interactions in vivo. Plant Physiol. 2016;171: 727–758. doi:10.1104/pp.16.00470

3. Brückner A, Polge C, Lentze N, Auerbach D, Schlattner U. Yeast two-hybrid, a powerful tool for systems biology. Int J Mol Sci. 2009;10: 2763–2788. doi:10.3390/ijms10062763

4. Goodson ML, Farboud B, Privalsky ML. An improved high throughput protein-protein interaction assay for nuclear hormone receptors. Nucl Recept Signal. 2009;5: e002. doi:10.1621/nrs.05002

5. Vincentelli R, Luck K, Poirson J, Polanowska J, Abdat J, Blémont M, et al. Quantifying domain-ligand affinities and specificities by high-throughput holdup assay. Nat Methods. 2015;12: 787–793. doi:10.1038/nmeth.3438

6. Hall MD, Yasgar A, Peryea T, Braisted JC, Jadhav A, Simeonov A, et al. Fluorescence polarization assays in high-throughput screening and drug discovery: A review. Methods Appl Fluoresc. 2016;4: 022001. doi:10.1088/2050-6120/4/2/022001

7. Roehrl MHA, Wang JY, Wagner G. A general framework for development and data analysis of competitive high-throughput screens for small-molecule inhibitors of protein-protein interactions by fluorescence polarization. Biochemistry. 2004;43: 16056–16066. doi:10.1021/bi048233g

8. Roehrl MHA, Wang JY, Wagner G. Discovery of small-molecule inhibitors of the NFAT-calcineurin interaction by competitive high-throughput fluorescence polarization screening. Biochemistry. 2004;43: 16067–16075. doi:10.1021/bi048232o

9. Donato R. Functional roles of S100 proteins, calcium-binding proteins of the EF-hand type. Biochim Biophys Acta - Mol Cell Res. 1999;1450: 191–231. doi:10.1016/S0167-4889(99)00058-0

10. Chen H, Xu C, Jin Q, Liu Z. S100 protein family in human cancer. Am J Cancer Res. 2014;4: 89–115.

11. Marenholz I, Heizmann CW, Fritz G. S100 proteins in mouse and man: From evolution to function and pathology (including an update of the nomenclature). Biochem Biophys Res Commun. 2004;322: 1111–1122. doi:10.1016/j.bbrc.2004.07.096

bioRxiv preprint doi: https://doi.org/10.1101/718155; this version posted July 29, 2019. The copyright holder for this preprint (which was not certified by peer review) is the author/funder, who has granted bioRxiv a license to display the preprint in perpetuity. It is made available under aCC-BY 4.0 International license.

12. Bresnick AR, Weber DJ, Zimmer DB. S100 proteins in cancer HHS Public Access. Nat Rev Cancer. 2015;15: 96–109. doi:10.1038/nrc3893

13. Bresnick AR. S100 proteins as therapeutic targets. Biophys Rev. 2018;10: 1617–1629. doi:10.1007/s12551-018-0471-y

14. Donato R. S100: A multigenic family of calcium-modulated proteins of the EF-hand type with intracellular and extracellular functional roles. Int J Biochem Cell Biol. 2001;33: 637–668. doi:10.1016/S1357-2725(01)00046-2

15. Wheeler LC, Anderson JA, Morrison AJ, Wong CE, Harms MJ. Conservation of Specificity in Two Low-Specificity Proteins. Biochemistry. 2018;57: 684–695. doi:10.1021/acs.biochem.7b01086

16. Hartman KG, Vitolo MI, Pierce AD, Fox JM, Shapiro P, Martin SS, et al. Complex formation between s100b protein and the p90 ribosomal S6 kinase (RSK) in malignant melanoma is calcium-dependent and inhibits extracellular signalregulated kinase (ERK)-mediated phosphorylation of RSK. J Biol Chem. 2014;289: 12886–12895. doi:10.1074/jbc.M114.561613

17. Inman KG, Yang R, Rustandi RR, Miller KE, Baldisseri DM, Weber DJ. Solution NMR structure of S100B bound to the high-affinity target peptide TRTK-12. J Mol Biol. 2002;324: 1003–1014. doi:10.1016/S0022-2836(02)01152-X

18. Kiss B, Duelli A, Radnai L, Kekesi KA, Katona G, Nyitray L. Crystal structure of the S100A4-nonmuscle myosin IIA tail fragment complex reveals an asymmetric target binding mechanism. Proc Natl Acad Sci. 2012;109: 6048–6053. doi:10.1073/pnas.1114732109

19. Biri-Kovács B, Kiss B, Vadászi H, Gógl G, Pálfy G, Török G, et al. Ezrin interacts with S100A4 via both its N- and C-terminal domains. PLoS One. 2017;12: e0177489. doi:10.1371/journal.pone.0177489

20. Sakane K, Nishiguchi M, Denda M, Yamagchi F, Magari M, Kanayama N, et al. Identification and characterization of a centrosomal protein, FOR20 as a novel S100A6 target. Biochem Biophys Res Commun. 2017;491: 980–985. doi:10.1016/j.bbrc.2017.07.161

21. Bousova K, Herman P, Vecer J, Bednarova L, Monincova L, Majer P, et al. Shared CaM- and S100A1-binding epitopes in the distal TRPM4 N terminus. FEBS J. 2018;285: 599–613. doi:10.1111/febs.14362

22. van Dieck J, Fernandez-Fernandez MR, Veprintsev DB, Fersht AR. Modulation of the oligomerization state of p53 by differential binding of proteins of the S100 family to p53 monomers and tetramers. J Biol Chem. 2009;284: 13804–13811. doi:10.1074/jbc.M901351200

bioRxiv preprint doi: https://doi.org/10.1101/718155; this version posted July 29, 2019. The copyright holder for this preprint (which was not certified by peer review) is the author/funder, who has granted bioRxiv a license to display the preprint in perpetuity. It is made available under aCC-BY 4.0 International license.

23. Wilder PT, Lin J, Bair CL, Charpentier TH, Yang D, Liriano M, et al. Recognition of the tumor suppressor protein p53 and other protein targets by the calcium-binding protein S100B. Biochim Biophys Acta - Mol Cell Res. 2006;1763: 1284–1297. doi:10.1016/j.bbamcr.2006.08.024

24. Lin J, Blake M, Tang C, Zimmer D, Rustandi RR, Weber DJ, et al. Inhibition of p53 Transcriptional Activity by the S100B Calcium-binding Protein. J Biol Chem. 2002;276: 35037–35041. doi:10.1074/jbc.m104379200

25. Rustandi RR, Baldisseri DM, Weber DJ. Structure of the negative regulatory domain of p53 bound to S100B(ββ). Nat Struct Biol. 2000;7: 570–574. doi:10.1038/76797

26. Lee Y-T, Dimotrova YN, Schneider G, Ridenour WB, Bhattacharya S, Soss SE, et al. Structure of the S100A6 complex with a fragment from the C-terminal domain of Siah-1 interacting protein: A novel mode for S100 protein target recognition. Biochemistry. 2008;47: 10921–10932. doi:10.1021/bi801233z

27. Gógl G, Alexa A, Kiss B, Katona G, Kovács M, Bodor A, et al. Structural Basis of Ribosomal S6 Kinase 1 (RSK1) Inhibition by S100B Protein. J Biol Chem. 2015;291: 11–27. doi:10.1074/jbc.m115.684928

28. Ecsédi P, Kiss B, Gógl G, Radnai L, Buday L, Koprivanacz K, et al. Regulation of the Equilibrium between Closed and Open Conformations of Annexin A2 by N-Terminal Phosphorylation and S100A4-Binding. Structure. 2017;25: 1195–1207. doi:10.1016/j.str.2017.06.001

29. Zimmer DB, Eubanks JO, Ramakrishnan D, Criscitiello MF. Evolution of the S100 family of calcium sensor proteins. Cell Calcium. 2013;53: 170–179. doi:10.1016/j.ceca.2012.11.006

30. Wheeler LC, Donor MT, Prell JS, Harms MJ. Multiple evolutionary origins of ubiquitous Cu2+ and Zn2+ binding in the s100 protein family. PLoS One. 2016;11: e0164740. doi:10.1371/journal.pone.0164740

31. Aguilar D, Aviles FX, Querol E, Sternberg MJE. Analysis of phenetic trees based on metabolic capabilites across the three domains of life. J Mol Biol. 2004;340: 491–512. doi:10.1016/j.jmb.2004.04.059

32. Sokal RR, Michener CD. A Statistical Method for Evaluating Systematic Relationships. Univ Kansas Sci Bull. 1958;38: 1409–1438.

33. Gógl G, Biri-Kovács B, Durbesson F, Jane P, Nomine Y, Kostmann C, et al. Rewiring of RSK–PDZ Interactome by Linear Motif Phosphorylation. J Mol Biol. 2019;431: 1234–1249. doi:10.1016/j.jmb.2019.01.038

34. Park S-H, Raines RT. Fluorescence polarization assay to quantify protein-protein interactions. Methods Mol Biol. 2015;261: 161–165. doi:10.1385/1-59259-762-9:161

bioRxiv preprint doi: https://doi.org/10.1101/718155; this version posted July 29, 2019. The copyright holder for this preprint (which was not certified by peer review) is the author/funder, who has granted bioRxiv a license to display the preprint in perpetuity. It is made available under aCC-BY 4.0 International license.

35. Rossi AM, Taylor CW. Analysis of protein-ligand interactions by fluorescence polarization. Nat Protoc. 2011;6: 365–387. doi:10.1038/nprot.2011.305

36. Shimamoto S, Kubota Y, Yamaguchi F, Tokumitsu H, Kobayashi R. Ca 2+ /S100 proteins act as upstream regulators of the chaperone-associated ubiquitin ligase chip (c terminus of hsc70-interacting protein). J Biol Chem. 2013;288: 7158–7168. doi:10.1074/jbc.M112.436758

37. Liu Y, Myrvang HK, Dekker L V. Annexin A2 complexes with S100 proteins: Structure, function and pharmacological manipulation. Br J Pharmacol. 2015;172: 1664–1676. doi:10.1111/bph.12978

38. Fernandez-Fernandez MR, Rutherford TJ, Fersht AR. Members of the S100 family bind p53 in two distinct ways. Protein Sci. 2008;17: 1663–1670. doi:10.1110/ps.035527.108

39. Schwaller B. cytosolic Ca2+ Buffers. Cold Spring Harb Perspect Biol. 2010;2: a004051. doi:10.1016/B978-0-12-374145-5.00120-0

40. Spratt DE, Barber KR, Marlatt NM, Ngo V, Macklin JA, Xiao Y, et al. A Subset of Calcium-binding S100 Proteins Show Preferential Heterodimerization. FEBS J. 2019;286: 1859–1876. doi:10.1111/febs.14775

41. Wang S, Song R, Wang Z, Jing Z, Wang S, Ma J. S100A8/A9 in inflammation. Front Immunol. 2018;9: 1298. doi:10.3389/fimmu.2018.01298

42. Harms MJ, Thornton JW. Evolutionary biochemistry: Revealing the historical and physical causes of protein properties. Nat Rev Genet. 2013;14: 559–571. doi:10.1038/nrg3540

43. Kiss B, Ecsédi P, Simon M, Nyitray L. Isolation and Characterization of S100 Protein-Protein Complexes. Methods Mol Biol. 2019;1929: 325–338. doi:10.1007/978-1-4939-9030-6_21

44. Anthis NJ, Clore GM. Sequence-specific determination of protein and peptide concentrations by absorbance at 205 nm. Protein Sci. 2013;22: 851–858. doi:10.1002/pro.2253

45. Kuipers BJH, Gruppen H. Prediction of molar extinction coefficients of proteins and peptides using UV absorption of the constituent amino acids at 214 nm to enable quantitative reverse phase high-performance liquid chromatography-mass spectrometry analysis. J Agric Food Chem. 2007;55: 5445–5451. doi:10.1021/jf070337l

46. Madeira F, Park YM, Lee J, Buso N, Gur T, Madhusoodanan N, et al. The EMBL-EBI search and sequence analysis tools APIs in 2019. Nucleic Acids Res. 2019;1: gkz268. doi:10.1093/nar/gkz268

47. Katoh K, Rozewicki J, Yamada KD. MAFFT online service: multiple sequence alignment, interactive sequence choice and visualization. Brief Bioinform. 2017; 1–7. doi:10.1093/bib/bbx108

bioRxiv preprint doi: https://doi.org/10.1101/718155; this version posted July 29, 2019. The copyright holder for this preprint (which was not certified by peer review) is the author/funder, who has granted bioRxiv a license to display the preprint in perpetuity. It is made available under aCC-BY 4.0 International license.

48. Silvestro D, Michalak I. RaxmlGUI: A graphical front-end for RAxML. Org Divers Evol. 2012;12: 335–337. doi:10.1007/s13127-011-0056-0

49. Le SQ, Gascuel O. An improved general amino acid replacement matrix. Mol Biol Evol. 2008;25: 1307–1320. doi:10.1093/molbev/msn067

50. Hammer Ø, Harper DAT, Ryan PD, Ryan DD, Ryan PD. PAST palenotological statistics. Palaentologia Electron. 2011;4: 5–7. doi:10.1016/j.bcp.2008.05.025

bioRxiv preprint doi: https://doi.org/10.1101/718155; this version posted July 29, 2019. The copyright holder for this preprint (which was not certified by peer review) is the author/funder, who has granted bioRxiv a license to display the preprint in perpetuity. It is made available under aCC-BY 4.0 International license.

name	region	sequence	modification
fp53	p53 (17-56)	GSCETFSDLWKLLPENNVLSPLPSQAMDDLMLSPDDIEQWFTE	fluorescein-izothiocianate
fRSK1	RSK1 (689-735)	GSCQDLQLVKGAMAATYSALNSSKPTPQLKPIESSILAQRRVRKLPSTTL	fluorescein-izothiocianate
fNMIIA	NMIIA (1894-1937)	CRKLQRELEDATETADAMNREVSSLKNKLRRGDLPFVVPRRMARK	fluorescein-izothiocianate
fMDM4	MDM4 (25-43)	NQVRPKLPLLKILHAAGAQ	N-terminal carboxyfluorescein
fCapZ	CapZ (265-276)	TRTKIDWNKILS	N-terminal carboxyfluorescein
fNCX1	NCX1 (254-265)	RRLLFYKYVYKR	N-terminal carboxyfluorescein
fTRPM4	TRPM4 (129-147)	VLQTWLQDLLRRGLVRAAQ	N-terminal carboxyfluorescein
fSIP	SIP (188-202)	SEGLMNVLKKIYEDG	N-terminal carboxyfluorescein
fC-ERMAD	C-ERMAD (516-560)	GSCKRITEAEKNERVQRQLLTLSSELSQARDENKRTHNDIIHNENMRQG	Alexa Fluoro 568 C_5 maleimide
p53	p53 (1-60)	GSMEEPQSDPSVEPPLSQETFSDLWKLLPENNVLSPLPSQAMDDLMLSPDDI EQWFTEDPGP	None (free N- and C-terminus)
NMIIA	NMIIA (1894-1937)	YRKLQRELEDATETADAMNREVSSLKNKLRRGDLPFVVPRRMARK	None (free N- and C-terminus)
MDM4	MDM4 (25-43)	NQVRPKLPLLKILHAAGAQ	None (free N- and C-terminus)
CapZ	CapZ (265-276)	TRTKIDWNKILS	None (free N- and C-terminus)
NCX1	NCX1 (254-265)	RRLLFYKYVYKR	None (free N- and C-terminus)
TRPM4	TRPM4 (129-147)	VLQTWLQDLLRRGLVRAAQ	None (free N- and C-terminus)
SIP	SIP (188-202)	SEGLMNVLKKIYEDG	None (free N- and C-terminus)
C-ERMAD	C-ERMAD (516-586)	GSCKRITEAEKNERVQRQLLTLSSELSQARDENKRTHNDIIHNENMRQGRDK YKTLRQIRQGNTKQRIDEFEAL	None (free N- and C-terminus)
FOR20	FOR20 (1-48)	GSMATVAELKAVLKDTLEKKGVLGHLKARIRAEVFNALDDDREPRPSLSH	None (free N- and C-terminus)
FOP	FOP (1-48)	GSYAATAAAVVAEEDTELRDLLVQTLENSGVLNRIKAELRAAVFLALEEQ	None (free N- and C-terminus)

Table 1. Peptides used in this study

The dissociation constant deduced from direct (d) and competitive (c) experiments

	fp53 (d)	p53 (c)	fNMIIA (d)	NMIIA (c)	fCapZ (d)	CapZ (c)	fNCX1 (d)	NCX1 (c)	fSIP (d)	SIP (c)	FOR20 (c)
S100A1	41±11	> 200	0.033±0.0062	0.004±0.001	8.9±2.0	5.2±1.7	2.6±0.14	2.6±0.56	> 200	N.D.	0.50±0.25
S100A2	2.9±0.08	5.2±0.39	0.057±0.0038	0.013±0.0022	> 200	N.D.	5.5±0.37	> 200	102±40	> 200	0.27±0.03
S100A3	7.6±0.44	7.7±1.9	5.5±1.0	E.A.	> 200	N.D.	25±2.5	> 200	> 200	N.D.	29±5.6
S100A4	0.85±0.04	2.1±0.23	0.026±0.0065	0.0088±0.0025	> 200	N.D.	15±0.62	> 200	42±5.2	11±2.7	2.0±0.20
S100A5	26±2.4	67±23	5.8±0.67	2.9±0.51	4.7±0.28	5.4±0.84	4.6±0.22	5.2±1.1	42±3.2	40±7.8	1.9±0.53
S100A6	0.68±0.020	2.2±0.090	0.58±0.07	0.21±0.04	> 200	N.D.	27±1.8	> 200	8.7±0.48	20±1.1	0.007±0.0018
S100A7	> 200	N.D.	13.1±1.4	E.A.	> 200	N.D.	30±2.1	E.A.	> 200	N.D.	5.9±0.54
S100A8	> 200	N.D.	> 200	N.D.	> 200	N.D.	56±5.0	E.A.	> 200	N.D.	> 200
S100A9	> 200	N.D.	> 200	N.D.	> 200	N.D.	20±3.2	> 200	> 200	N.D.	> 200
S100A10	48±2.9	> 200	> 200	N.D.	> 200	N.D.	53±6.6	> 200	> 200	N.D.	> 200
S100A11	10±0.72	12±2.4	49±14	E.A.	> 200	N.D.	52±2.9	E.A.	> 200	N.D.	> 200
S100A12	76±11	N.D.	> 200	N.D.	> 200	N.D.	170±63	E.A.	> 200	N.D.	> 200
S100A13	35±10	> 200	> 200	N.D.	> 200	N.D.	87±14	E.A.	> 200	N.D.	> 200
S100A14	> 200	N.D.	98±127	E.A.	> 200	N.D.	71±7.5	E.A.	> 200	N.D.	63±30
S100A15	> 200	N.D.	17±1.5	E.A.	> 200	N.D.	28±3.4	E.A.	> 200	N.D.	17±2.1
S100A16	79±8.9	N.D.	> 200	N.D.	> 200	N.D.	> 200	N.D.	> 200	N.D.	> 200
S100B	33±3.2	> 200	4.7±0.25	2.9±0.31	2.3±0.13	1.8±0.23	7.7±0.95	> 200	> 200	N.D.	0.25±0.050
S100G	> 200	N.D.	21±1.9	E.A.	> 200	N.D.	24±1.7	E.A.	> 200	N.D.	3.8±1.1
S100P	0.17±0.01	0.54±0.040	0.99±0.11	0.14±0.03	11±1.4	4.1±0.73	4.0±0.23	> 200	38±3.2	> 200	1.2±0.13
S100Z	> 200	N.D.	> 200	N.D.	> 200	N.D.	11±0.45	E.A.	> 200	N.D.	> 200
	fTRPM4 (d)	**TRPM4 (c)**	**fMDM4 (d)**	**MDM4 (c)**	**fC-ERMAD (d)**	**C-ERMAD (c)**	**fRSK1 (d)**	**RSK1-CTKD (c)**	**MK2 (c)**	**MNK1 (c)**	**FOP (c)**
S100A1	0.38±0.061	> 200	91±14	35±10	> 200	N.D.	4.8±0.72	> 200	15±4.6	> 200	0.35±0.14
S100A2	1.0±0.062	1.1±0.23	49±10	53±16	15±0.62	5.4±0.57	5.1±0.53	> 200	4.5±1.0	18±4.2	0.081±0.019
S100A3	0.91±0.052	3.4±0.45	> 200	N.D.	> 200	N.D.	> 200	N.D.	> 200	> 200	0.27±0.13
S100A4	5.9±0.36	35±113	> 200	N.D.	11±0.73	6.1±0.80	8.5±0.89	> 200	> 200	24±3.5	0.048±0.010
S100A5	0.60±0.051	2.3±0.71	61±5.4	65±7.5	> 200	N.D.	> 200	N.D.	> 200	> 200	0.56±0.20
S100A6	1.4±0.081	8.4±2.0	> 200	N.D.	> 200	N.D.	8.7±0.81	> 200	> 200	6.7±0.53	0.0056±0.0050
S100A7	> 200	N.D.	> 200	N.D.	> 200	N.D.	> 200	N.D.	E.A.	E.A.	> 200
S100A8	3.8±0.57	13±4.4	> 200	N.D.	> 200	N.D.	> 200	N.D.	N.D.	> 200	> 200
S100A9	21±7.3	> 200	> 200	N.D.	> 200	N.D.	> 200	N.D.	N.D.	> 200	> 200
S100A10	17±1.9	125±25	> 200	N.D.	> 200	N.D.	> 200	N.D.	> 200	> 200	> 200
S100A11	2.4±0.12	106±11	> 200	N.D.	> 200	N.D.	> 200	N.D.	> 200	> 200	> 200
S100A12	> 200	N.D.	> 200	N.D.	> 200	N.D.	> 200	N.D.	N.D.	> 200	> 200
S100A13	> 200	N.D.	> 200	N.D.	> 200	N.D.	> 200	N.D.	N.D.	N.D.	> 200
S100A14	12±5.6	> 200	> 200	N.D.	> 200	N.D.	> 200	N.D.	E.A.	E.A.	> 200
S100A15	> 200	N.D.	> 200	N.D.	> 200	N.D.	> 200	N.D.	E.A.	E.A.	> 200
S100A16	> 200	N.D.	> 200	N.D.	> 200	N.D.	> 200	N.D.	N.D.	> 200	> 200
S100B	16±25	> 200	0.20±0.04	0.15±0.04	> 200	N.D.	2.8±0.47	1.2±0.86	3.2±0.73	> 200	1.2±0.53
S100G	> 200	N.D.	> 200	N.D.	> 200	N.D.	> 200	N.D.	E.A.	E.A.	> 200
S100P	0.93±0.24	> 200	> 200	N.D.	> 200	N.D.	4.5±0.47	> 200	2.7±0.47	2.5±0.38	0.066±0.0049
S100Z	> 200	N.D.	> 200	N.D.	> 200	N.D.	> 200	N.D.	N.D.	N.D.	> 200

Table 2. Quantitative characterization of interactions between S100 proteins and their selected partners by FP (N.D.: not determined; E.A.: experimental artifact).

bioRxiv preprint doi: https://doi.org/10.1101/718155; this version posted July 29, 2019. The copyright holder for this preprint (which was not certified by peer review) is the author/funder, who has granted bioRxiv a license to display the preprint in perpetuity. It is made available under aCC-BY 4.0 International license.

measurement	T / K	N	Reference N	K_d / μM	ΔH / (kJ/mol)	-TΔS (kJ/mol)
S100A6-FOP	310	0.44 ± 0.002	Previously unknown	0.088 ± 0.0073	-73 ± 0.58	31
S100B-CapZ	310	0.44 ± 0.002 0.343 ± 0.002	1 [17]	3.9 ± 0.39 0.94 ± 0.03	-15 ± 0.37 -3.3 ± 0.67	-17 -33
S100A1-NCX1	310	1.1 ± 0.013	1 [15]*	6.4 ± 0.58	-35 ± 0.80	4.0
S100A5-TRPM4	310	0.89 ± 0.0037	Previously unknown	1.4 ± 0.089	-24 ± 0.21	-10
C-ERMAD-S100A4	310	1.9 ± 0.055	1.86 [19]	35 ± 4.4	-26 ± 2.2	0,047
S100A5-SIP	310	0.92 ± 0.24	1.5 [26]*	21 ± 20	-4.1 ± 2.5	-24
S100A1-NMIIA	298	0.49 ± 0.0017	0.5 [18]*	0.009 ± 0.005	36 ± 0.34	-82
S100B-MDM4	310	0.52 ± 0.039 0.53 ± 0.038	1 [23]	0.71 ± 0.036 0.63 ± 0.081	-186 ± 142 111 ± 148	150 -148
S100B-RSK1	298	0.49 ± 0.0086	0.5 [27]	12 ± 1.4	-32 ± 1.4	-60
S100P-p53	310	0.28 ± 0.0053	Previously unknown	1.7 ± 0.19	-63 ± 1.9	29

Table 3. Quantitative characterization of interactions between S100 proteins and their selected partners by ITC.

*These interactions were measured with a different S100 paralog

bioRxiv preprint doi: https://doi.org/10.1101/718155; this version posted July 29, 2019. The copyright holder for this preprint (which was not certified by peer review) is the author/funder, who has granted bioRxiv a license to display the preprint in perpetuity. It is made available under aCC-BY 4.0 International license.

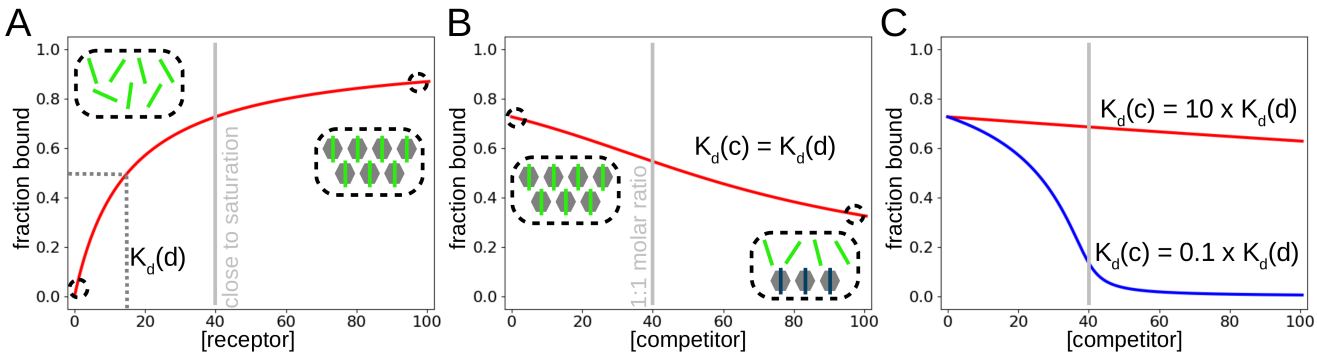

Fig 1. **A:** Fluorescence polarization/anisotropy experiments can be performed with direct and competitive titrations. In direct assay, the concentration of the protein of interest is increased in the presence of tracer amount of labeled peptide. Upon complex formation, the hydrodynamic radius of the tracer increases causing slower rotation and therefore lower depolarization of the emitted light. In the direct assay, one can measure the minimal and maximal polarization values, a dissociation constant and importantly, an optimal concentration can be easily determined for competitive assays, which is usually the concentration corresponding to 60-80% saturation. **B:** in a competitive assay, the concentration of the protein of interest is set to this concentration and one can titrate the reaction mixture with a competitor. The competition results in increased level of free labeled peptide and consequently high depolarization of the emitted light. **C:** competitive FP is not affected by the presence of a labeling group in the peptide (unbiased) and has a high dynamic range (approximately 2 orders of magnitudes around the dissociation constant of the probe). At high concentrations, it can be also used to determine the stoichiometry of the interaction for strong interactions.

bioRxiv preprint doi: https://doi.org/10.1101/718155; this version posted July 29, 2019. The copyright holder for this preprint (which was not certified by peer review) is the author/funder, who has granted bioRxiv a license to display the preprint in perpetuity. It is made available under aCC-BY 4.0 International license.

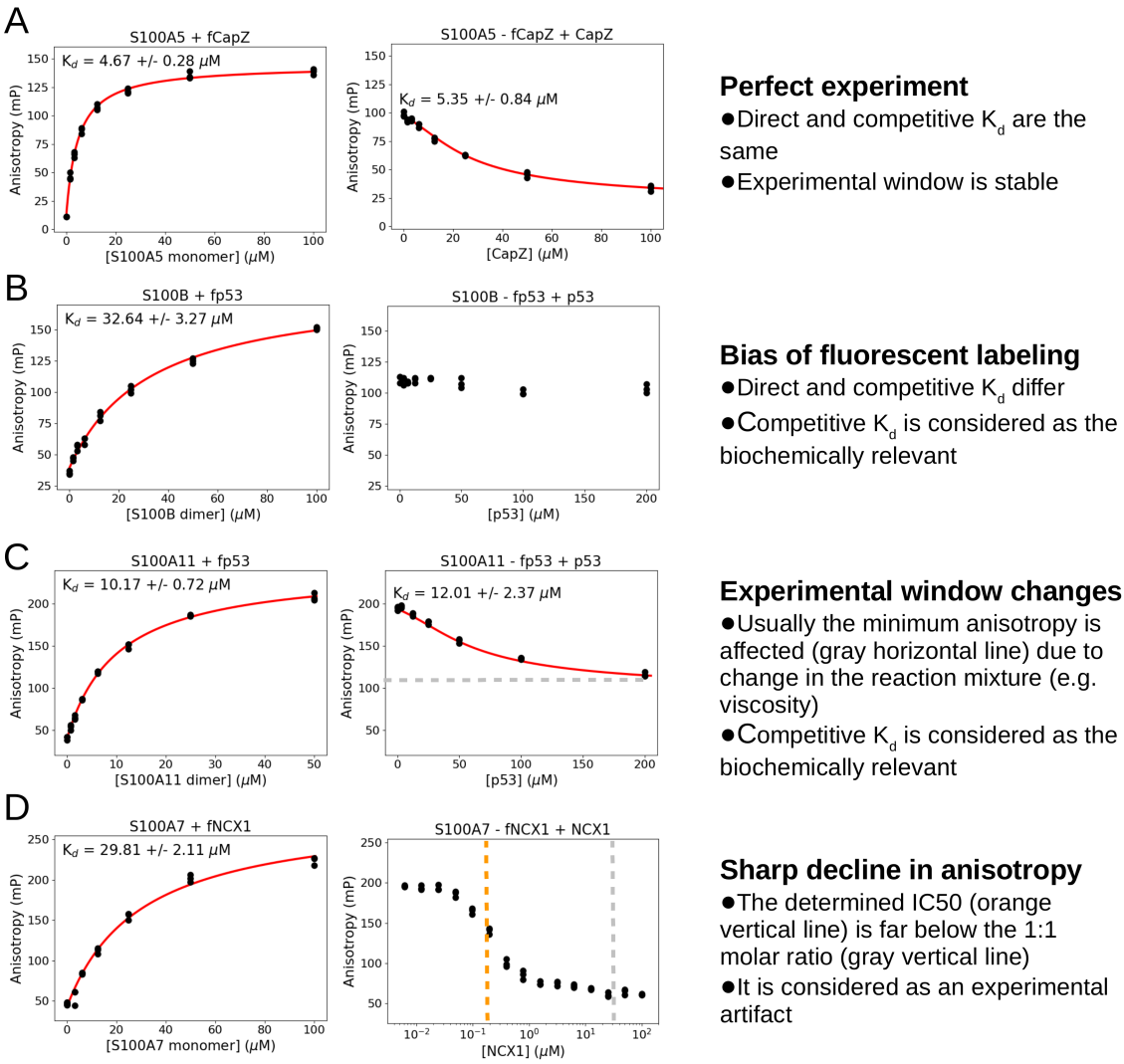

Fig 2. **A:** in "perfect experiments", the experimental window is stable and the dissociation constants match between the (cognate) probe and the competitor. **B:** as often occurs, fluorescent labeling can alter the binding affinity, resulting in false positive interaction partners in direct FP experiments. In other cases, the effect is softer and it only causes a dimming effect on the biochemical constant. **C:** the reliable experimental window can be different in a competitive experiment. If the change is not extreme, the competitive K_d can be considered (with caution) as the relevant biochemical constant. **D:** in some cases, a rapid decline can be observed in the polarization. In this case, the experimentally determined IC50 value should not be used as a dissociation constant. This phenomena can be explained by a competitor induced biophysical transition, e.g. aggregation or precipitation. In this final case, it is very important to redetermine the concentrations of the receptor and the competitor and to repeat the experiment at different receptor concentrations to properly discriminate the stoichiometric molar ratio from the observed IC50 value.

bioRxiv preprint doi: https://doi.org/10.1101/718155; this version posted July 29, 2019. The copyright holder for this preprint (which was not certified by peer review) is the author/funder, who has granted bioRxiv a license to display the preprint in perpetuity. It is made available under aCC-BY 4.0 International license.

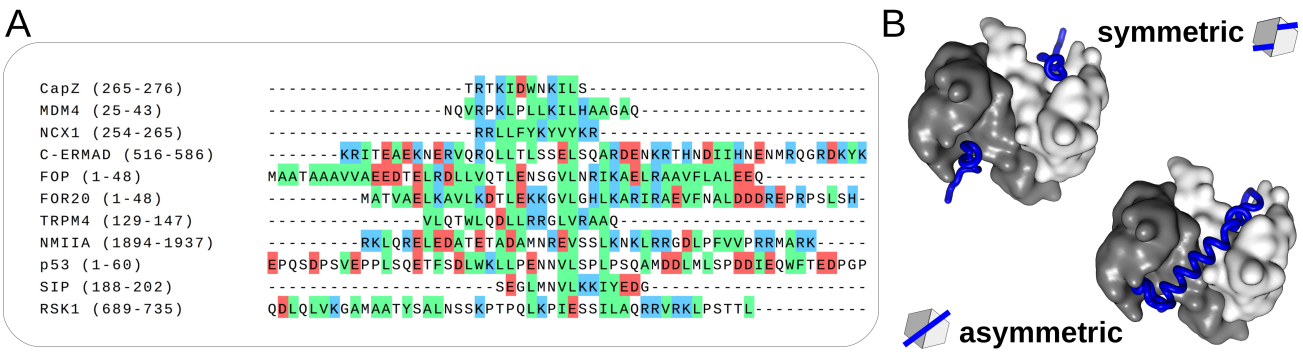

Fig 3 **A:** multiple short linear motifs are recognized by S100 family members, however no consensus binding motif can be defined for the protein family, as indicated here by the sequence alignment of several S100 binding motifs. Though it is noteworthy that hydrophobic residues (green) are preferred, basic residues are also welcome in some cases. **B:** S100 proteins act as dimers and are capable of interacting in two distinct ways with other proteins. On the left, a symmetric complex is shown, where one S100 dimer interacts with two peptides (S100B-CapZ, [17]). By contrast, a single interacting partner can bind to one S100 dimer asymmetrically, as it is shown on the right side (S100A4-NMIIA, [18]).

bioRxiv preprint doi: https://doi.org/10.1101/718155; this version posted July 29, 2019. The copyright holder for this preprint (which was not certified by peer review) is the author/funder, who has granted bioRxiv a license to display the preprint in perpetuity. It is made available under aCC-BY 4.0 International license.

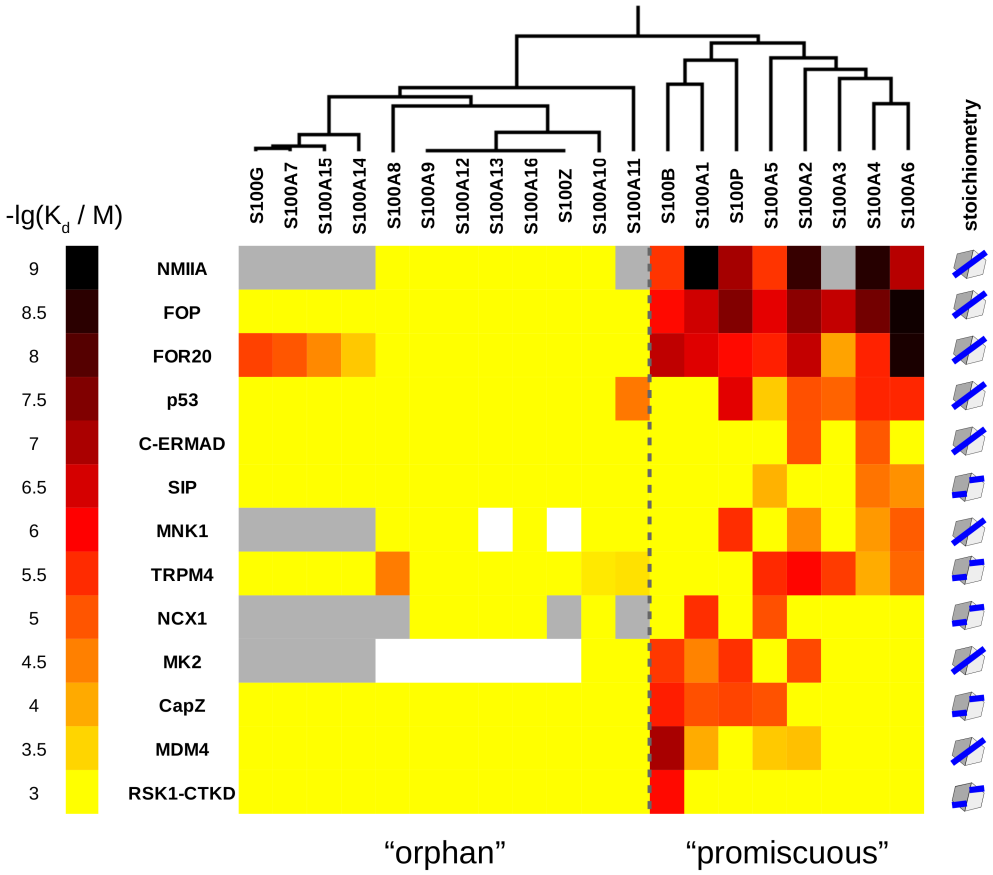

Fig 4. The determined dissociation constants are depicted as a heatmap representing the specificity-map of the S100ome. Hierarchical clustering, based on functional relationships, divided the S100ome into two different groups, one of them consists of low(er) specificity and/or more promiscuous S100 proteins ('promiscuous'), while the other one contains high(er) specificity and/or less promiscuous members of the family ('orphan'). White and grey fields indicate non-determined interactions and cases with experimental artifacts, respectively. Stoichiometry (1:1 or 2:1 to 1 S100 dimer) is also shown for all ligands at the end of each rows.